Electronic Supplementary Information

Porous current collector cleaner enables thin cathode electrolyte interphase on $LiCoO_2$ for stable high-voltage cycling

Zhong Xu Lu[a], Ke Wen Mu[a], Zhi Yong Zhang[a], Qin Luo[a], Yan Hong Yin*[a], Xian Bin Liu[a], Ye Sheng Li[a], Yong Lei*[b] and Zi Ping Wu*[a]

[a] Ganzhou Key Laboratory of Advanced Metals and Functional Materials, School of Materials Science and Engineering, Jiangxi University of Science and Technology (JXUST), Ganzhou 341000, P. R. China.

[b] Fachgebiet Angewandte Nanophysik, Institut für Physik & ZMN MacroNano (ZIK), Technische Universität Ilmenau, Ilmenau 98693, Germany.

* Corresponding author E-mail: yinyanhong@jxust.edu.cn (Y. H. Yin); yong.lei@tu-ilmenau.de (Y. Lei); wuziping724@jxust.edu.cn (Z. P. Wu)

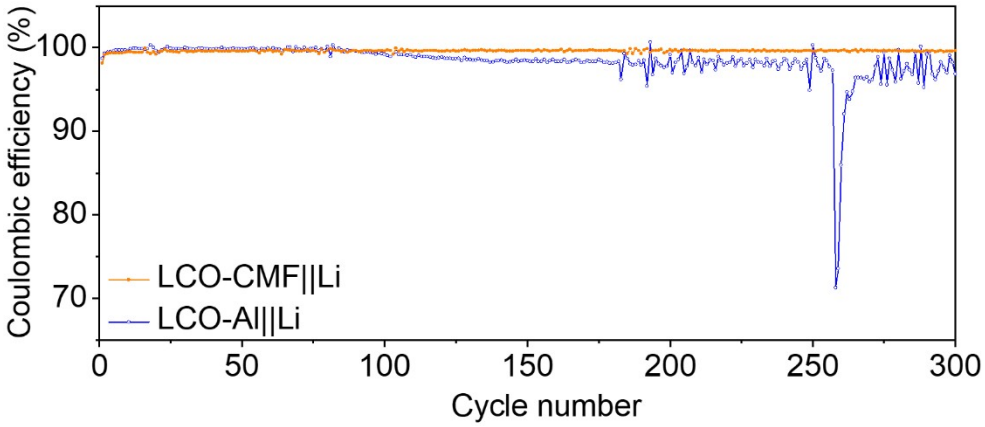

Fig. S1 The Coulombic efficiency of LCO-Al||Li and LCO-CMF||Li at different cycles

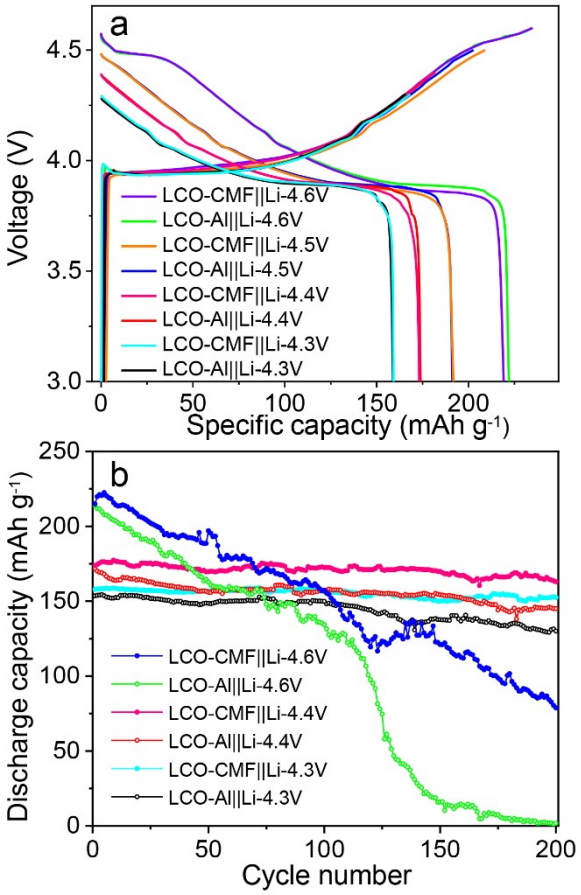

Fig. S2 The first discharging/charging curves (a) at 0.1 C and cycles performance (b) of LCO-Al||Li and LCO-CMF||Li with different cutoff voltage at 0.5C

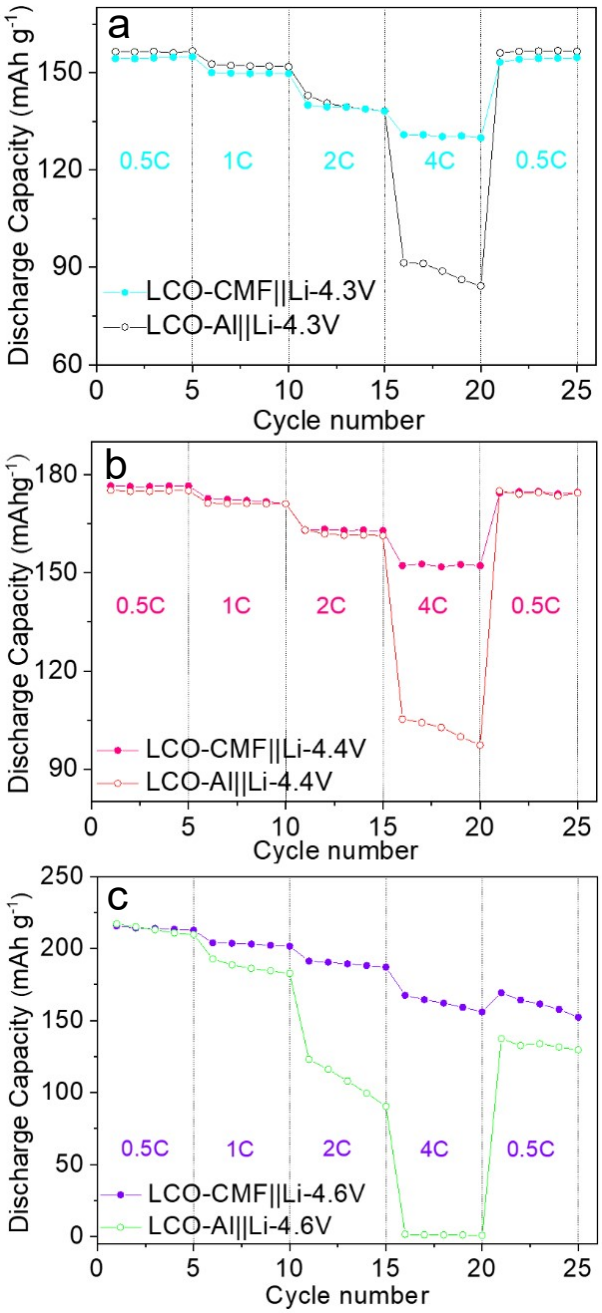

Fig. S3 The rate capability of LCO-Al||Li and LCO-CMF||Li with mass loading of 5 mg cm^{-2} at cutoff voltage of 4.3 V (a), 4.4 V (b) and 4.6 V (c)

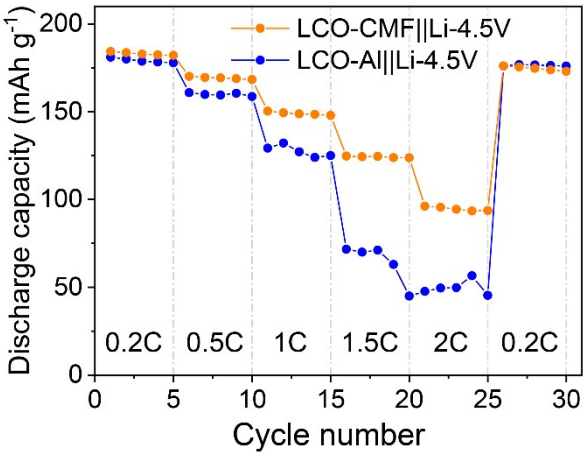

Fig. S4 The rate capability of LCO-Al||Li and LCO-CMF||Li with a high mass loading of 16 mg cm^{-2} at cutoff voltage of 4.5 V

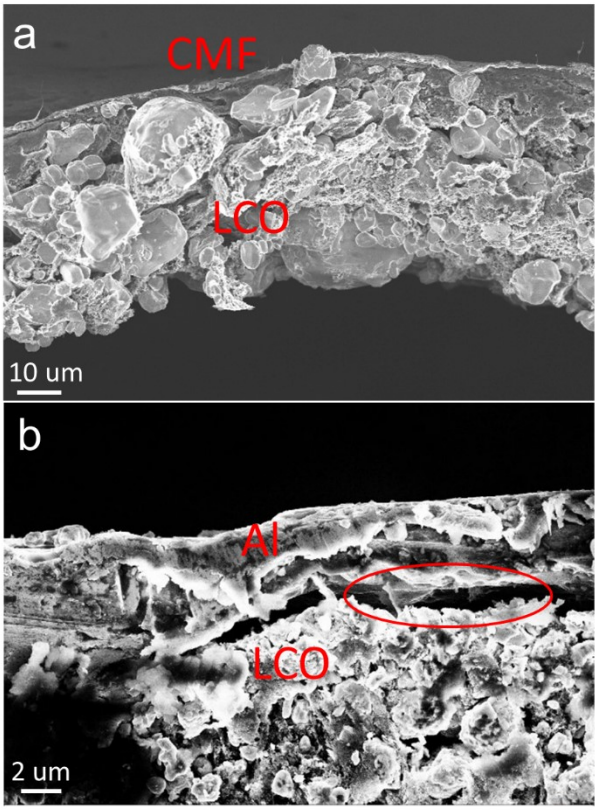

Fig. S5 The typical cross-section images of LCO-CMF (a) and LCO-Al (b) electrodes

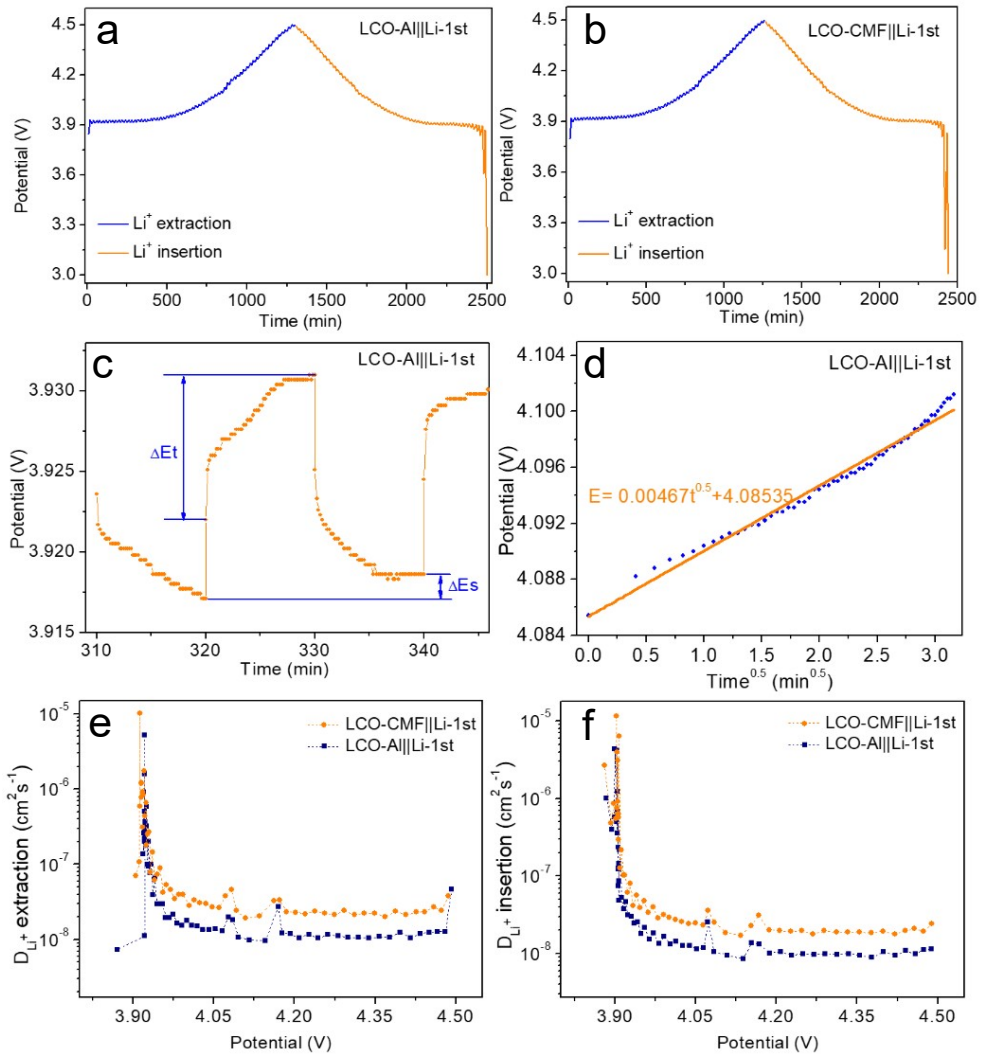

Fig. S6 The first cycle galvanostatic intermittent titration technique (GITT) curves at 0.1 C of LCO-Al (a) and LCO-CMF (b), E vs t(c)□in a single step, linear relationship (d) between E and $t^{0.5}$ during a typical titration and extraction (e) and insertion (f) of D_{Li^+} values calculated from the GITT curves for the cells based different current collectors.

To study the Li^+ diffusivity of LCO using different Al foil and CMF, the GITT experiment was performed on electrode LCO-Al during the first Li^+ insertion/extraction processes at room temperature. The Li^+ diffusion coefficient ($^{D_{Li}}$) can be determined using the Fick's second law with equation (1):[1, 2]

$$D_{Li} = \frac{4}{\pi}\left(\frac{m_B V_m}{M_B S}\right)^2 \left[\frac{\Delta Es}{t\left(\frac{dEt}{d\sqrt{t}}\right)}\right]^2 \quad (t \ll \frac{L2}{D_{Li}}) \qquad (1)$$

where M_B is the molar weight of LCO, S is the real surface area of LCO, V_m is molar volume of LCO, m_B is mass weight of LCO, t is titration time, ΔEt is potential variation during pulse, and ΔEs is variation in equilibrium potential. Since potential was linearly proportional to $t^{0.5}$ during single titration (Fig. S18c), equation (1) was simplified as equation (2):

$$D_{Li} = \frac{4}{\pi t}\left(\frac{m_B V_m}{M_B S}\right)^2 \left(\frac{\Delta Es}{\Delta Et}\right)^2 \left(t \ll \frac{L2}{D_{Li}}\right) \quad (2)$$

Based on the calculation, the LCO-Al||Li and LCO-CMF||Li cell variation tendencies of D_{Li} during the Li^+ extraction/insertion processes are shown in Fig. S5e, f.

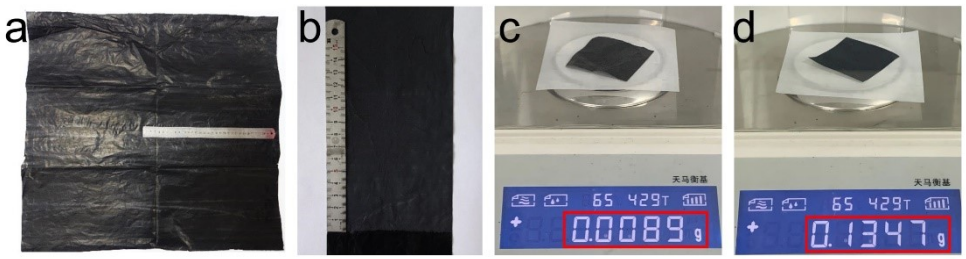

Fig. S7 The photograph of CMF (a), LCO-CMF (b), and the weight of the CMF (c) and LCO-CMF (d) with area of ~5×5 cm^2

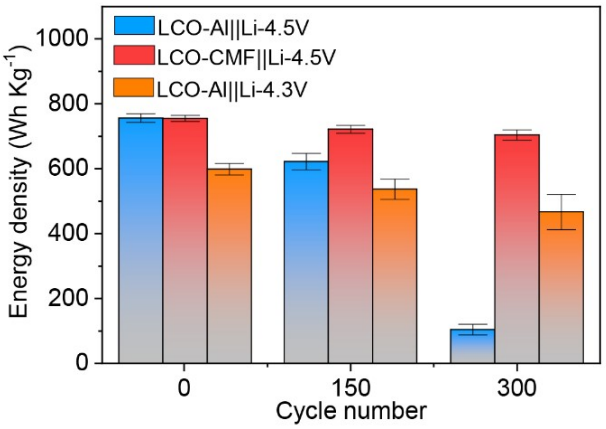

Fig. S8 The energy density of LCO-Al||Li with cutoff voltage of 4.3 V, LCO-Al||Li with cutoff voltage of 4.5 V and LCO-CMF||Li with cutoff voltage of 4.5 V, the energy densities were calculated based on weight of the LCO

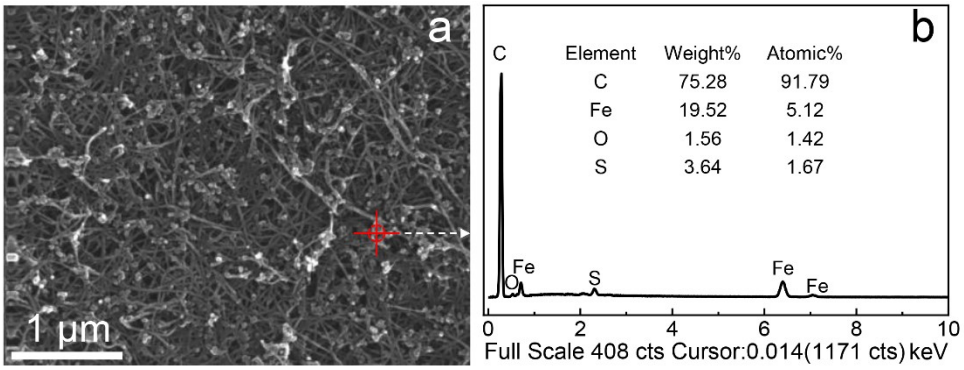

Fig. S9 The typical SEM image of the as-prepared CMF (a) and the EDS result (b) of the selected area in (a)

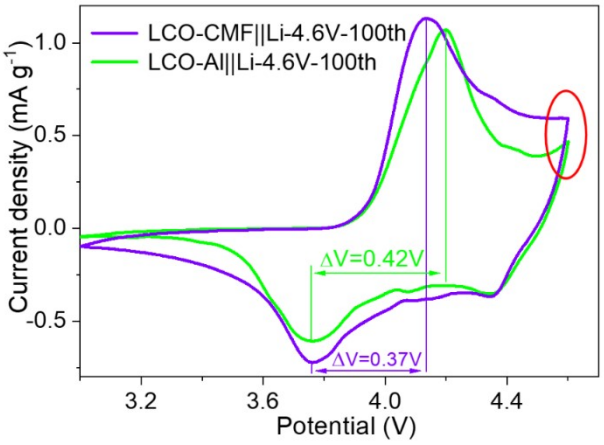

Fig. S10 The CV curves of LCO-Al||Li and LCO-CMF||Li with cutoff voltage of 4.6 V after 100 cycles

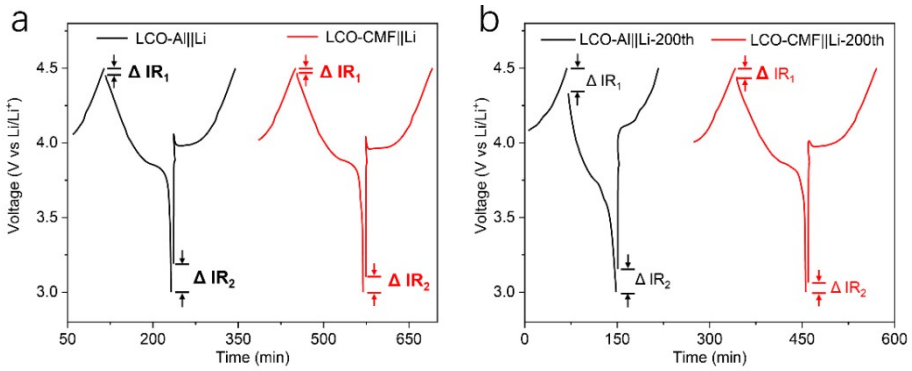

Fig. S11 Galvanostatic charge/discharge of the LTO-Al||Li and LTO-CMF||Li at first (a) and 200 cycles (b) with a C-rate of 0.5 C

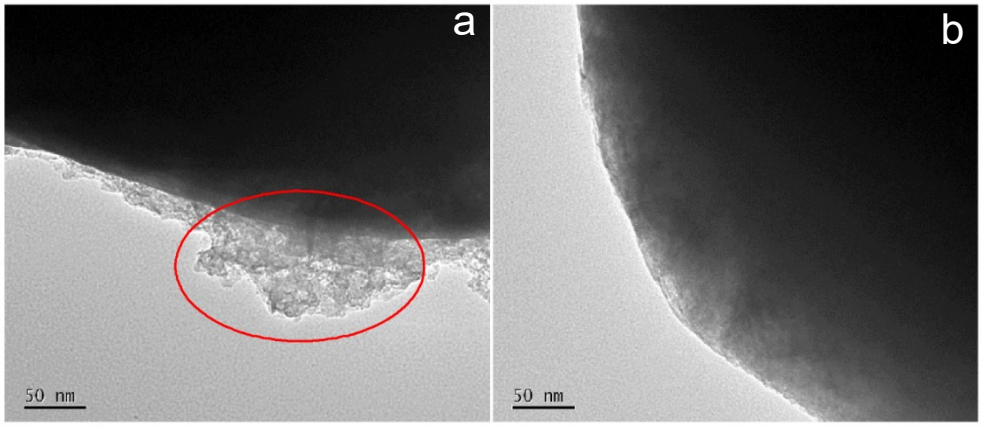

Fig. S12 The HRTEM images of surface of LCO on Al foil (a) and CMF (b) after 200 cycles

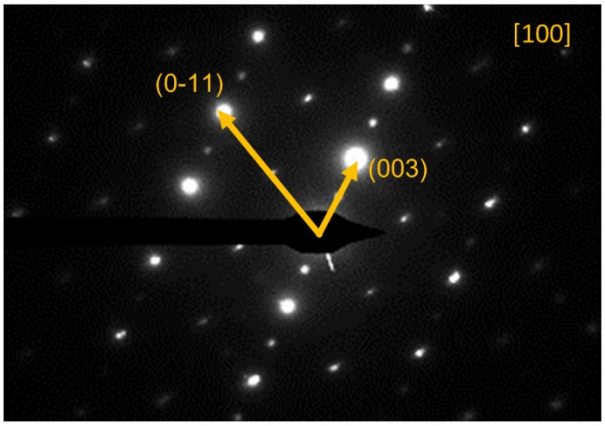

Fig. S13 The SAED of LCO peeled off from LCO-CMF electrode after 200 cycles

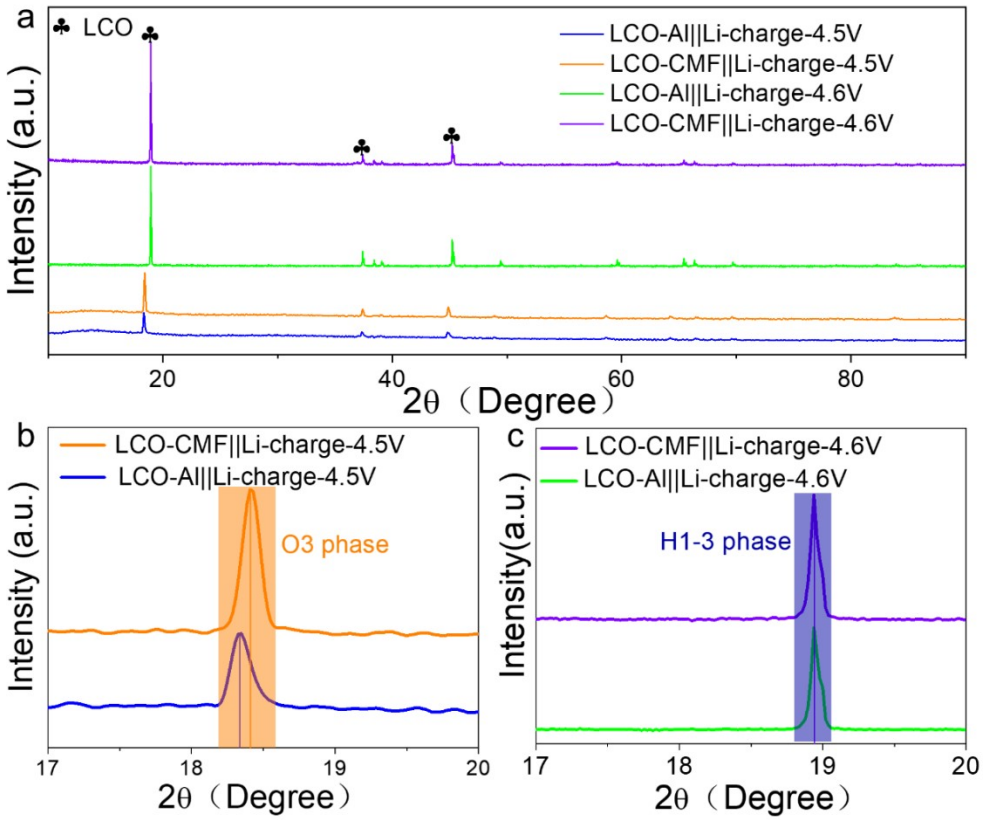

Fig. S14 The XRD patterns of LCO peeled off from LCO-Al and LCO-CMF with cutoff voltage of 4.5 V and 4.6 V after 200 cycles (a), the enlarged XRD patterns of different electrode after cycles with cutoff voltage of 4.5 V (b) and 4.6 V (c)

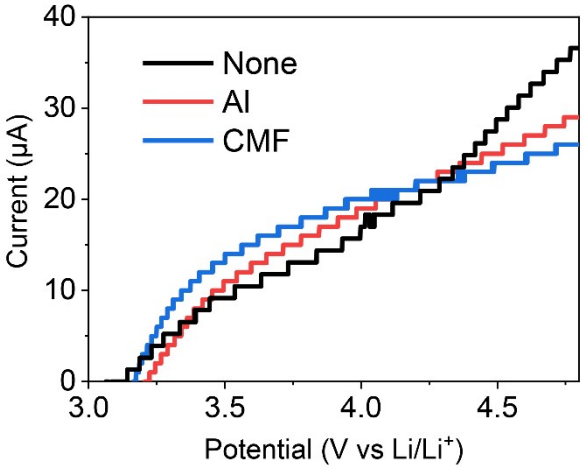

Fig. S15 The linear sweep voltammetry of electrolyte ($LiPF_6$ in EC/DEC) in a coin cell with current collector tested voltage from 3.0 V to 5.0 V, the scanning rate is 0.1 mV s^{-1}

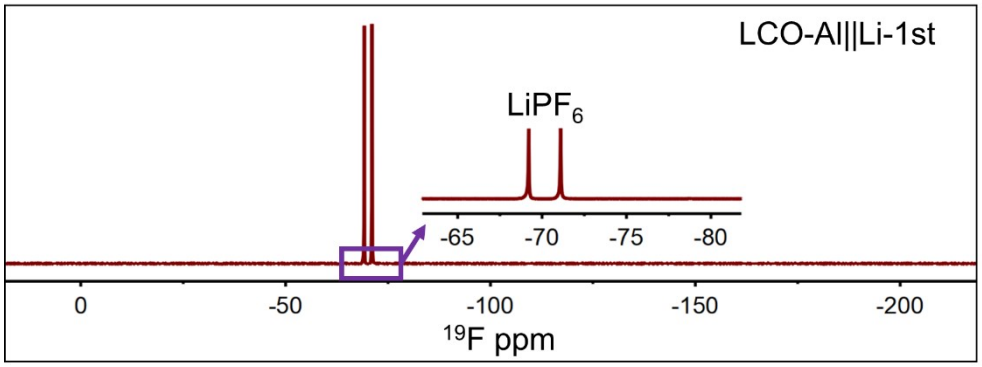

Fig. S16 Typical ^{19}F NMR spectrum of electrolyte from LCO-Al||Li after first cycles

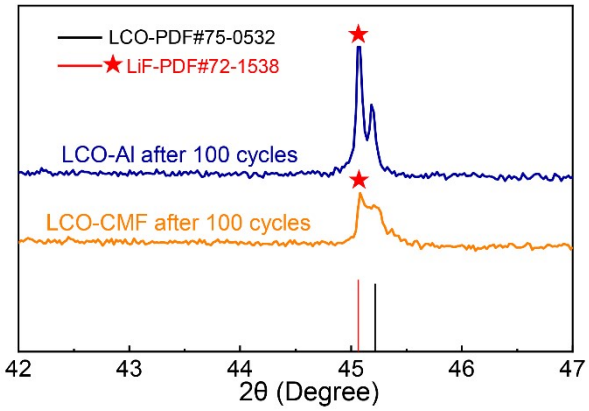

Fig. S17 The magnified XRD patterns of LCO for different electrodes after cycles near the strongest peaks

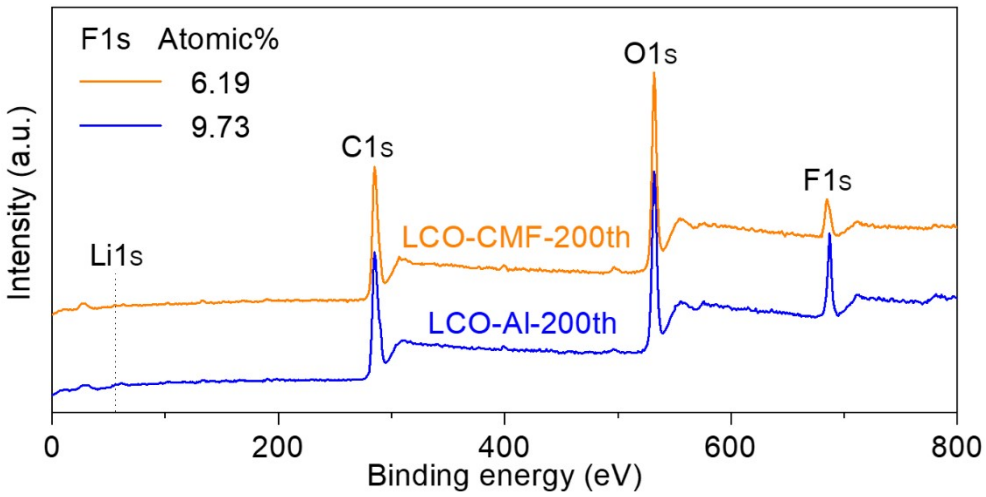

Fig. S18 The XPS patterns of LCO from the surface of LCO-Al and LCO-CMF after 200 cycles

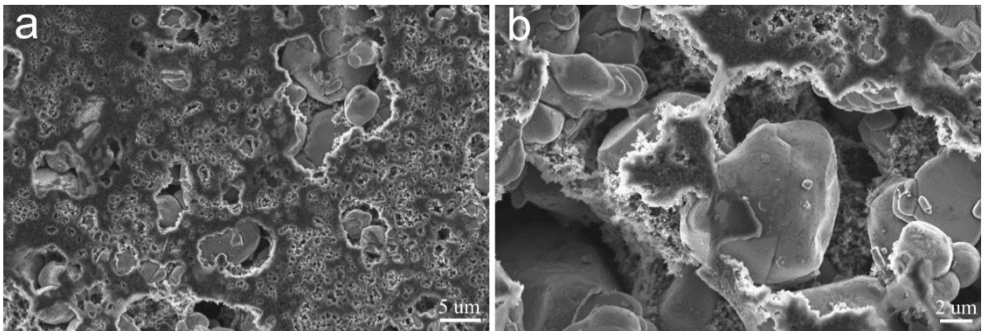

Fig. S19 The typical SEM images of the LCO surface (a, b) near the current collector side from the LCO-Al electrode

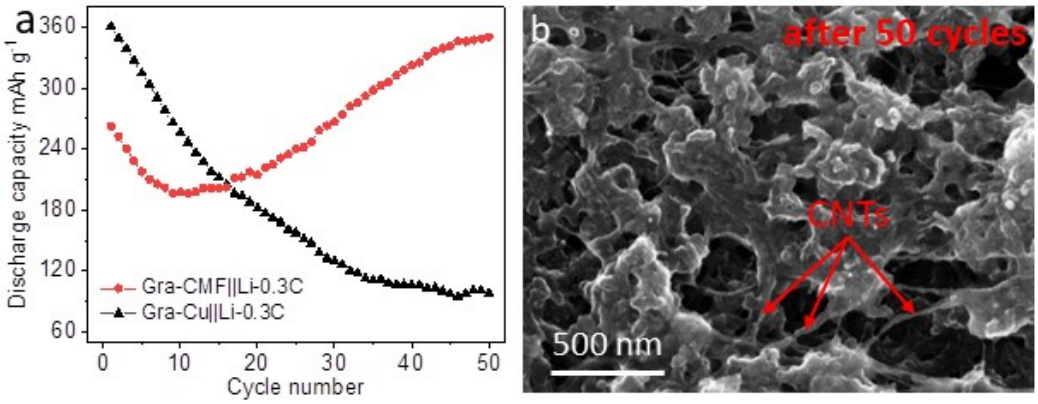

Fig. S20 The cycle performances (a) of Graphite-Cu||Li and Graphite-CMF||Li at 0.5C and the typical SEM image (b) of CMF from Graphite-CMF after 50 cycles

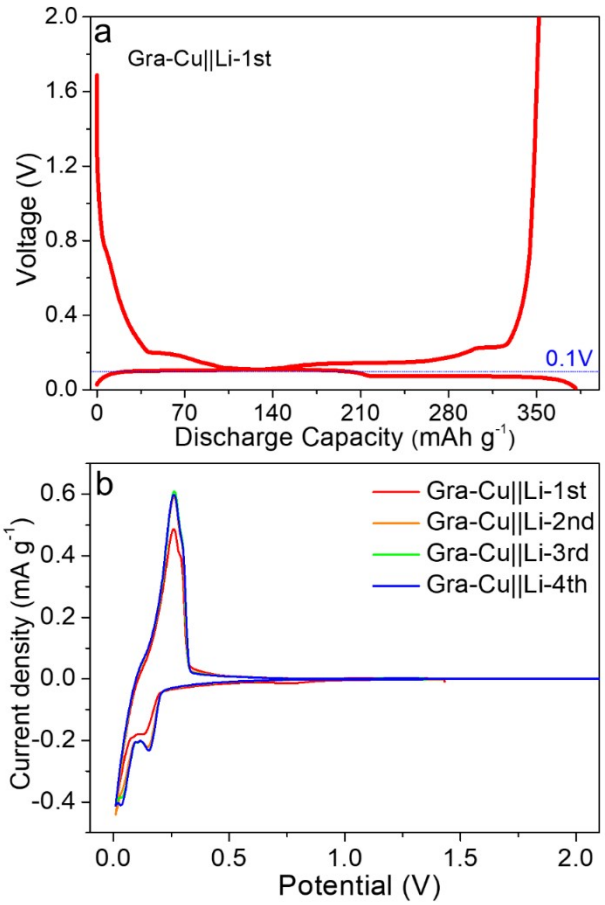

Fig. S21 The discharging/charging curves of Graphite-Cu||Li at first cycles (a), and CV curves (b) of Graphite-Cu||Li cell at different cycles

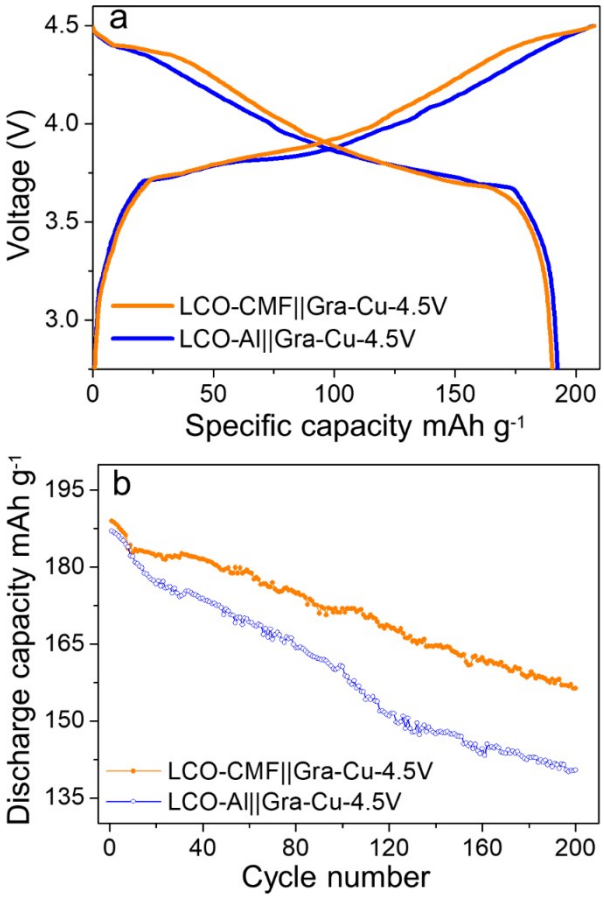

Fig. S22 The discharging/charging curves (a) and cycle performances (b) of LCO-Al||Gra-Cu and LCO-CMF||Gra-Cu pouch cells with cutoff voltage of 4.5 V

Table S1 The R_s and R_f of LCO-Al||Li and LCO-CMF||Li at different cycles from EIS results

	LCO-Al||Li-5th	LCO-CMF||Li-5th	LCO-Al||Li-200th	LCO-CMF||Li-200th
R_s（Ω）	3	3.3	4.2	4.8
R_f（Ω）	164	115	212	172

Table S2 The contents of LCO on Al foil and CMF before and after cycles

Element	C (At%)	Co (At%)	O (At%)	F (At%)	Total (%)
LCO-Al after 200 cycles	12.21	75.39	8.17	4.23	100
LCO-CMF after 200 cycles	15.28	71.62	10.39	2.71	100
LCO-Al before cycle	10.61	78.92	10.47	---	100

Table S3 The sheet resistance of different CMF using for loading LCO before and after cycles

Resistance	R1 $\Omega\square^{-1}$	R2 $\Omega\square^{-1}$	R3 $\Omega\square^{-1}$	$R_{average}$
CMF before cycle	5.4	5.6	5.4	5.5
CMF after 200 cycles	6.2	6.4	6.8	6.5

Table S4 Comparison of electrochemical performances based on CMF with other previous LCO-based batteries

Strategy	Configuration	Capacity retention (%)	Areal loading (mg cm^{-2})	Voltage (V)	Energy density Wh Kg^{-1}	Ref.
$Li_{1.5}Al_{0.5}Ti_{1.5}(PO_4)_3$ coating	LCO||Li	88 (100th)	3	3.0-4.6	306	3
nitriles and fluoroethylene carbonate +1 M $LiPF_6$ EC/ EMC	LCO||Li	75 (300th)	6	3.0-4.6	431	4
Mg doping	LCO||Li	84 (100th)	3	3.0-4.6	304	5
LHCE+1 M $LiPF_6$ EC/ EMC	LCO||Li	84 (300th)	13.5	3.0-4.5	530	6
PVDF–PVAC	LCO||Li	85 (200th)	1.5	3.0-4.5	180	7
PDES-CPE	LCO||Li	82 (100th)	1	3.0-4.6	152	8
Mg、La doping Ti coating	LCO||Li	83 (300th)	12	3.0-4.5	514	9
Lithium-Aluminum-Phosphate coating	LCO||Li	89 (200th)	3-4	3.0-4.6	375	10
La、Al doping	LCO||Li LCO||Gra	96 (50th) 74 (60th)	10 10	3.0-4.5 2.5-4.5	488 500	11
Al、Ti doping Mg coating	LCO||Li LCO||MCMB	75 (200th) 78 (200th)	1.5 7	3.0-4.6 3.0-4.5	211 480	12
Li、Al doping F coating	LCO||Li LCO||Gra	82 (200th) 76 (70th)	12.6 12.6	3.0-4.6 3.0-4.6	572 568	13
Mg、Al、Ti doping	LCO||Li LCO||Gra	86 (100th) 79 (70th)	3-4 15	3.0-4.6 3.0-4.55	340 652	14
Se coating	LCO||Li LCO||Gra	85 (120th) 80 (250th)	3 17	3.0-4.62 3.0-4.57	364 634	15
$LiNi_{0.5}Mn_{1.5}O_4$ coating	LCO||Li LCO||Gra	72 (50th) 81 (400th)	5 10	3.0-4.6 3.0-4.45	431 421	16
$Li_{1.5}Al_{0.5}Ge_{1.5}(PO_4)_3$ coating	LCO||Gra	83 (200th)	9	2.5-4.45	446	17
$LiNi_{0.45}Al_{0.05}Mn_{0.5}O_2$ coating	LCO||Gra	87 (150th)	10	3.0-4.48	458	18
$Li_4Ti_5O_{12}$ coating	LCO||Gra	89 (150th)	12	2.8-4.5	449	19
cathode prelithiation	LCO||Gra-SiO	76 (100th)	18.5	3.0-4.2	442	20
DMSE+1 M $LiPF_6$ EC/DMC/EMC	LCO||Gra	66 (100th)	15.4	3.0-4.5	588	21
CMF as current collector	LCO||Li LCO||Gra	94(300th) 82(200th)	5 16	3.0-4.5 3.0-4.4	651 645	This Work

Note: The energy density is calculated based on the weight of cathode electrode.

References

1 W. Weppner and R. A. Huggins, Determination of the kinetic parameters of mixted-conducting electrodes and application to the system Li_3Sb, *J. Electrochem. Soc.*, 1977, **124**, 1569-1578.

2 Q. F. Fu, R. J. Li, X. Z. Zhu, G. S. Liang, L. J. Luo, Y. J. Chen, C. F. Lin and X. S. Zhao, Design, synthesis and lithium-ion storage capability of $Al_{0.5}Nb_{24.5}O_{62}$, *J. Mater. Chem. A*, 2019, **7**, 19862-19872.

3 Y. Wang, Q. H. Zhang, Z. C. Xue, L. F. Yang, J. Y. Wang, F. Q. Meng, Q. H. Li, H. Y. Pan, J. N. Zhang, Z. Jiang, W. L. Yang, X. Q. Yu, L. Gu and H. Li, An in situ formed surface coating layer enabling $LiCoO_2$ with stable 4.6 V high-voltage cycle performances, *Adv. Energy Mater.*, 2020, **15**, 2001413-1-10.

4 X. R. Yang, M. Lin, G. R. Zheng, J. Wu, X. S. Wang, F. C. Ren, W. G. Zhang, Y. Liao, W. M. Zhao, Z. G. Zhang, N. B. Xu, W. L. Yang and Y. Yang, Enabling stable high-voltage $LiCoO_2$ operation by using synergetic interfacial modification strategy, *Adv. Funct. Mater.*, 2020, **30**, 2004664-1-12.

5 Y. Y. Huang, Y.C. Zhu, H.Y. Fu, M.Y. Ou, C. C. Hu, S. J. Yu, Z. W. Hu, C. T. Chen, G. Jiang, H. K. Gu, H. Lin, W. Luo and Y. H. Huang, Mg-pillared $LiCoO_2$: towards stable cycling at 4.6 V, *Angew. Chem.*, 2021, **13**, 4732-4738.

6 X. D. Ren, X. H. Zhang, Z. Shadike, L. F. Zou, H. Jia, X. Cao, M. H. Engelhard, B. E. Matthews, C. M. Wang, B. W. Arey, X. Q. Yang, J. Liu, J. G. Zhang and W. Xu, Designing advanced in situ electrode/electrolyte interphases for wide temperature operation of 4.5 V Li||$LiCoO_2$ batteries, *Adv. Mater.*, 2020, **32**, 2004898-1-8.

7 X. R. Yu, L. L. Wang, J. Ma, X. W. Sun, X. H. Zhou and G. L. Cui, Selectively wetted rigid-flexible coupling polymer electrolyte enabling superior stability and compatibility of high-voltage lithium metal batteries, *Adv. Energy Mater.*, 2020, **10**, 1903939-1-9.

8 C. Wang, H. R. Zhang, S. M. Dong, Z. L. Hu, R. X. Hu, Z. Y. Guo, T. Wang, G. L. Cui andL. Q. Chen, High polymerization conversion and stable high-voltage chemistry underpinning an in situ formed solid electrolyte, *Chem. Mater.*, 2020, **32**, 9167-9175.

9 T. Tian, T. W. Zhang, Y. C. Yin, Y. H. Tan, Y. H. Song, L. L. Lu and H. B. Yao, Blow-spinning enabled

precise doping and coating for improving high voltage lithium cobalt oxide cathode performance, *Nano Lett.*, 2019, **20**, 677-685.

10 X. Wang, Q. Wu, S. Y. Li, Z. M. Tong, D. Wang, H. L. Zhuang, X. Y. Wang and Y. Y. Lu, Lithium-Aluminum-phosphate coating enables stable 4.6 V cycling performance of $LiCoO_2$ at room temperature and beyond, *Energy Stor. Mater.*, 2021, **37**, 67-76.

11 Q. Liu, X. Su, D. Lei, Y. Qin, J. G. Wen, F. M. Guo, Y. M. Wu, Y. C. Rong, R. H. Kou, X. H. Xiao, F. Aguesse, J. Bareño, Y. Ren, W. Q. Lu and Y. X. Li, Approaching the capacity limit of lithium cobalt oxide in lithium ion batteries via lanthanum and aluminium doping, *Nat. Energy*, 2018, **3**, 936-943.

12 L. L. Wang, J. Ma, C. Wang, X. R. Yu, R. Liu, F. Jiang, X. W. Sun, A. Du, X. H. Zhou and G. L. Cui, A novel bifunctional self-stabilized strategy enabling 4.6 V $LiCoO_2$ with excellent long-term cyclability and high-rate capability, *Adv. Sci.*, 2019, **19**, 1900355-1-11.

13 J. W. Qian, L. Liu, J. X. Yang, S. Y. Li, X. Wang, H. L. Luo and Y. Y. Lu, Electrochemical surface passivation of $LiCoO_2$ particles at ultrahigh voltage and its applications in lithium-based batteries, *Nat. Commun.*, 2018, **9**, 4918-1-11.

14 J. N. Zhang, Q. H. Li, C. Y. Ouyang, X. Q. Yu, M. Y. Ge, X. J. Huang, E. Y. Hu, C. Ma, S. F. Li, R. J. Xiao, W. L. Yang, Y. Chu, Y. J. Liu, H. G. Yu, X. Q. Yang, X. J. Huang, L. Q. Chen and H. Li, Trace doping of multiple elements enables stable battery cycling of $LiCoO_2$ at 4.6 V, *Nat. Energy*, 2019, **4**, 594-603.

15 Z. Zhu, H. Wang, Y. Li, R. Gao, X. H. Xiao, Q. P. Yu, C. Wang, I. Waluyo, J. X. Ding, A. Hunt and J. Li, A surface Se-substituted $LiCo[O_{2-\delta}Se_{\delta}]$ cathode with ultrastable high-voltage cycling in pouch full-cells, *Adv. Mater.*, 2020, **32**, 2005182-1-8.

16 P. P. Pang, Z. Wang, Y. M. Deng, J. M. Nan, Z. Y. Xing and H. Li, Delayed phase transition and improved cycling/thermal stability by spinel $LiNi_{0.5}Mn_{1.5}O_4$ modification for $LiCoO_2$ cathode at high voltages, *ACS Appl. Mater. Inter.*, 2020, **12,** 27339-27349.

17 Z. Y. Lia, A. J. Li, H. R. Zhang, F. H. Ning, W. X. Li, A. Zangiabadi, Q. Cheng, J. J. Borovilas, Y. J. Chen, H. J. Zhang, X. H. Xiao, C. Y. Ouyang, X. J. Huang, W. Lee, M. Y. Ge, Y. S. Chu, X. Y. Chuan and Y. Yang, Multi-scale stabilization of high-voltage $LiCoO_2$ enabled by nanoscale solid electrolyte coating, *Energy Stor. Mater.*, 2020, **29**, 71-77.

18 P. P. Pang, Z. Wang, X. X. Tan, Y. M. Deng, J. M. Nan, Z. Y. Xing and H. Li, $LiCoO_2$ @$LiNi_{0.45}Al_{0.05}Mn_{0.5}O_2$ as high-voltage lithium-ion battery cathode materials with improved cycling performance and thermal stability, *Electrochim. Acta*, 2019, **327**, 135018-1-9.

19 C. W. Wang, Y. Zhou, J. H. You, J. D. Chen, Z. Zhang, S. J. Zhang, C. G. Shi, W. D. Zhang, M. H. Zou, Y. Yu, J. T. Li, L. Y. Zeng, L. Huang and S. G. Sun, High-voltage $LiCoO_2$ material encapsulated in a $Li_4Ti_5O_{12}$ ultra-thin layer by high-speed solid-phase coating process, *ACS Appl. Energy Mater.*, 2020, **3**, 2593-2603.

20 X. X. Liu, Y. C. Tan, W. Y. Wang, C. H. Li, Z. W. Seh, L. Wang and Y. M. Sun, Conformal prelithiation nanoshell on $LiCoO_2$ enabling high energy lithium-ion batteries, *Nano Lett.*, 2020, **20**, 4558-4565.

21 X. Z. Zheng, T. Huang, G. H. Fang, Y. Pan, Q. H. Li and M. X. Wu. Di(methylsulfonyl) enthane: new electrolyte additive for enhancing $LiCoO_2$/electrolyte interface stability under high voltage, *ACS Appl. Mater. Inter.*, 2019, **11**, 36244-36251.